RSC Advances

PAPER

View Article Online
View Journal | View Issue

Cite this: *RSC Adv.*, 2020, **10**, 2150

Reduced graphene oxide-based highly sensitive pressure sensor for wearable electronics *via* an ordered structure and enhanced interlayer interaction mechanism†

Kemeng Zhou,[a] Changzhou Chen,[a] Min Lei,[a] Qian Gao,[a] Shuangxi Nie,[ab] Xinliang Liu*[ab] and Shuangfei Wang[ab]

Received 22nd October 2019
Accepted 28th December 2019

DOI: 10.1039/c9ra08653f

rsc.li/rsc-advances

Compressible carbon materials have promising applications in various wearable devices. However, it is still difficult to prepare a carbon material with superior mechanical properties, stable strain-electrical signal response, and high linear sensitivity. In this study, a compressible and conductive carbon aerogel with excellent properties is obtained by designing an ordered wavy layered structure with enhanced interactions between carbon layers. Bidirectional freezing is used to produce a wavy layered structure. Cellulose nanocrystals (CNC) and lignin play important roles in enhancing the interactions between reduced graphene oxide (rGO) layers. Due to the design of the carbon aerogel structure and interlayer interactions, the prepared carbon aerogel exhibits supercompressibility (up to 99% ultimate strain), excellent elasticity and fatigue resistance (91.3% height retention after 10 000 cycles at a strain of 30%), and stable strain-current response. Moreover, the carbon aerogel demonstrated an ultrahigh sensitivity of 190.94 kPa^{-1}, a wide linear range (within strain of 0–80%), and a low detection limit for pressure (0.875 Pa). These advantages suggest that this carbon aerogel has great application potential in wearable devices.

1. Introduction

Compressible carbon aerogels have attracted widespread attention for applications in wearable and lightweight electronic devices because of their chemical and thermal stability, good electrical conductivity, low density, and mechanical flexibility.[1,2] These devices usually require high mechanical properties such as elasticity, compressibility, fatigue resistance, *etc.*[3–5] However, most carbon aerogels suffer from poor mechanical strength as a result of the few connections and fragile joints in the networks.[6,7] Therefore, it is still a great challenge to prepare carbon aerogels with excellent mechanical performance.

Carbon aerogels have been fabricated *via* various methods including solvent thermal[8] or hydrothermal treatments,[9,10] chemical vapor deposition (CVD),[11] templating,[12] and freeze-casting.[13] Rational design of microstructure is an attractive research approach for improving the mechanical properties of carbon aerogels. For example, a honeycomb carbon aerogel prepared by directional freeze casting can withstand 50 000 times its own weight.[14] Due to the brittleness of carbon, when an aerogel is subjected to high-strain cycles of compression, the structure undergoes significant plastic deformation and the compressive strength decreases.[15] In order to improve the mechanical properties of carbon materials, a layered structure was developed using bidirectional freezing.[15,16] Carbon aerogels with layered structures prepared by bidirectional freezing have superior elasticity and good fatigue performance (25 000 cycles under 50% strain).[15]

In recent years, researchers have developed a range of multifunctional carbon aerogels using different materials such as carbon nanotubes (CNT),[17] graphene oxide (GO),[18] melamine foam/graphene,[19] polyurethane/carbon sponges,[20] and carbon nanofibers.[21] GO is one of the most attention-getting carbon-based materials due to its excellent conductivity, flexibility, and high strength.[22,23] However, van der Waals forces between graphene oxide nanosheets can cause severe agglomeration of nanosheets, resulting in graphene-oxide-based carbon aerogels with poor mechanical properties.[24] Studies have found that adding substances to enhance the interaction between graphene oxides can prevent or hinder the condensation polymerization of graphene oxide aerogels during carbonization reduction. For example, Peng *et al.* Prepared CNT/rGO–CNF carbon aerogel with excellent elasticity (94.6% height retention for 50 000 cycles) to enhance the interlayer interaction between reduced graphene oxide by adding CNFs and CNT.[25]

[a]*College of Light Industry and Food Engineering, Guangxi University, Nanning 530004, People's Republic of China. E-mail: xinliang.liu@hotmail.com*

[b]*Guangxi Key Laboratory of Clean Pulp & Papermaking and Pollution Control, Guangxi University, Nanning 530004, People's Republic of China*

† Electronic supplementary information (ESI) available. See DOI: 10.1039/c9ra08653f

In this study, carbon aerogels with super-compressibility, excellent elasticity, high fatigue resistance, and high sensitivity are fabricated by designing an orderly, wavy, layered structure and enhancing the interactions between carbon layers. The main factors responsible for these excellent properties are: (1) lignin and cellulose nanocrystals (CNC) can enhance inter sheet interactions between the GO sheets, and (2) the carbon aerogel microstructure is carefully designed using bidirectional freezing to produce a wavy layered structure. These features make carbon aerogels ideal candidates for wearable devices that detect bio-signals.

2. Experimental section

2.1 Materials

Nanocellulose (diameter of 10–20 nm and length of 0.5–2 mm) was purchased from Guilin Qihong Sci-Tech Co., Ltd. Sodium hydroxide was purchased from Nanjing Chemical Reagent Factory. Lignin was purchased from Sigma-Aldrich. Deionized water was used exclusively in this study.

2.2 Fabrication of lignin–CNC–GO suspension

GO was prepared by a modified Hummers'method.[26] 25 mL of sodium hydroxide solution (0.01 M) suspension containing GO, CNC and lignin was prepared. The concentration of GO in the suspension was 1 mg mL^{-1}, the concentration of CNC was 2 mg mL^{-1}/4 mg mL^{-1}/6 mg mL^{-1}, and the concentration of lignin is 0.4 mg mL^{-1}/2 mg mL^{-1}/4 mg mL^{-1}. To ensure adequate dispersion of the CNC and GO, the mixture was stirred at room temperature for 120 min and sonicated for 60 min. For comparison, CNC–GO and lignin–GO suspensions were also prepared by the same process.

2.3 Fabrication of aerogels

We refer to the bidirectional freezing method of Bai *et al.* For bidirectional freezing of the dispersion.[16] Both ends of a copper plate were inserted into liquid nitrogen to form a cooling stage. First, 6 mL of the above mixture was placed in a cubic plastic (15 mm × 15 mm × 40 mm) mold placed on the surface of the copper cooling plate. The bottom of the plastic mold was a 10° wedge made of PDMS. After they were frozen, the obtained lignin–CNC–GO nanocomposites were vacuum-dried for 48 h to obtain the aerogel. The preparation of aerogel Lig/CNC–GO was carried out in the same way with a lignin–CNC–GO suspension. CNC–GO and lignin–GO suspensions were used to prepare aerogels of CNC–GO and Lig–GO, respectively.

2.4 Fabrication of carbon aerogels

The aerogels were then carbonized in a tube furnace under N_2 atmosphere. The first stage of the process was carried out by heating the furnace from room temperature to 200 °C (5 °C min^{-1}) and holding that temperature for 2 h. Then, the aerogels were pyrolyzed by raising the temperature from 200 to 700 °C (3 °C min^{-1}) and holding that temperature for 2 h to obtain the carbon aerogels C–Lig/CNC–rGO, C–Lig–rGO, and C–CNC–rGO, respectively.

2.5 Characterizations

The unique microstructures of the samples were observed with transmission electron microscopy (TEM; Titan G2 ETEM, FEI) and scanning electron microscopy (SEM; Hitachi SU8220, Hitachi). Raman patterns were measured on a Raman spectrometer (LabRAM HR Evolution, HORIBA Jobin Yvon) operating with a 532 nm laser. X-ray diffraction (XRD) patterns were recorded on a SMARTLAB3KW diffractometer.

2.6 Mechanical and electrical testing

Compressive tests were carried out on a material testing machine (Instron 3367A, England) with a 500 N load cell, and samples were placed between two compression stages. The resistance of the carbon aerogel was measured using a multimeter (VC890D). The electrical current was recorded by using an electrochemical workstation (Autolab M204), and the applied voltage was 1.0 V.

2.7 Assembly and testing of the compressible sensor

The sensor was fabricated by fitting the carbon aerogel between two poly ethylene terephthalate (PET) substrates adhered with Cu electrodes. The real-time current signals were recorded by connecting the sensor to an electrochemical workstation. The current signal includes signals generated by compression, bending, and biological pulses. The pressure sensing tests were conducted by dropping water (50 μL) onto the sensor. The compression-induced resistance change was recorded on a multimeter (VC 890D).

3. Results and discussion

3.1 Fabrication of carbon aerogels and their characterizations

As shown in Fig. 1a, the compressible carbon aerogels were prepared by mixing, bidirectional freezing, freeze-drying, and carbonization. GO and CNC are highly hydrophilic and have good dispersibility in water. However, lignin is hydrophobic and does not disperse well in water. Therefore, GO, CNC, and lignin were dispersed in a 0.1 M sodium hydroxide solution. Cellulose can form hydrogen bonds both intra- and inter-molecularly. In particular, intra-molecular hydrogen bonds render glycosidic bonds incapable of rotation, which makes them rigid. In recent years, cellulose has been widely used as a reinforcing material to prepare high-performance biomass composite materials.[27] Therefore, cellulose can increase the mechanical strength of the carbon aerogel. In this work, cellulose was also used to prevent the re-stacking of GO during freeze casting and annealing.[28] Lignin, a natural polyphenolic material and a major by-product of the paper industry, has a higher carbon content (40–60 wt%) and can be converted into high-value carbonaceous materials. It is well known that lignin provides mechanical strength and rigidity to natural woody plants.[29] Some researchers have demonstrated the importance of lignin to the strength of natural wood tissue by observing the fiber lignification process (increasing the lignin content).[30] Bidirectional freezing results in the directed growth of ice crystals in the lamellar structure of

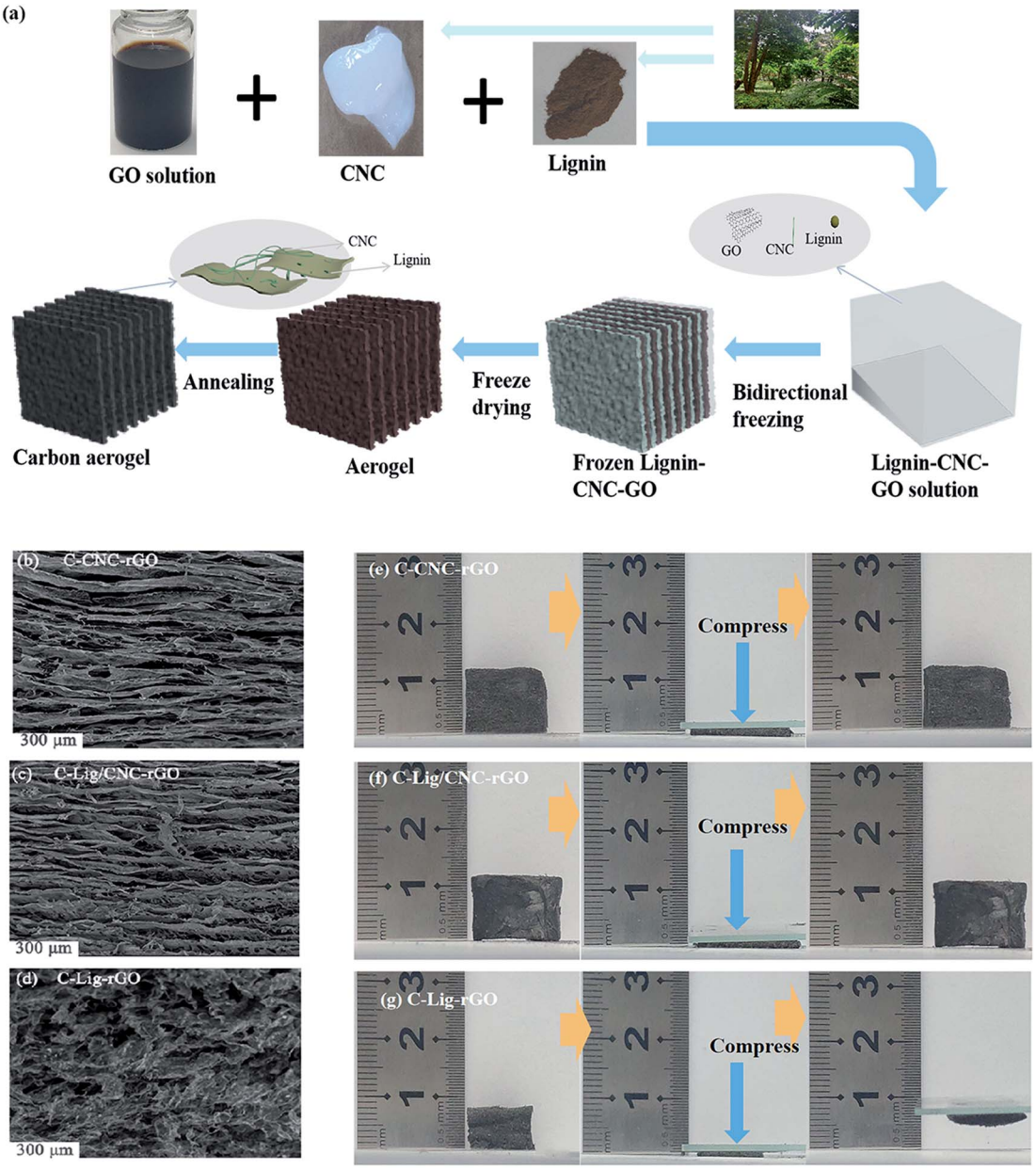

Fig. 1 (a) Schematic of carbon aerogel production. (b–d) SEM images of C–CNC–rGO, C–Lig/CNC–rGO, and C–Lig–rGO, respectively. (e–g) Digital photographs of the compression of C–CNC–rGO, C–Lig/CNC–rGO, and C–Lig–rGO, respectively.

the mixture.[16] As shown in Fig. S1,† slope angles was able to generate two temperature gradients: vertical and horizontal.[31] On cooling, the bottom end of the wedge has a lower temperature than the top end. Consequently, sample solidification started at the bottom and then propagated to the top of the wedge.[16] Thus, the initial formed ice nucleus would grow with the moved freezing points and form long-range paralleled ice columns. These paralleled ice columns simultaneously grow along vertical direction to form long-range paralleled ice lamellas.[16,31] During freeze-drying, ice is removed to produce aerogels with layered structures. These layers are well preserved during the carbonization process, as shown in Fig. 1b and c. The graphene oxide is reduced to form reduced graphene oxide during the carbonization process.

As shown in Fig. S2,† CNC–GO and Lig/CNC–GO before carbonization had good morphological retention. However, significant deformation of the Lig–GO sample occurred before carbonization. Morphological changes in the aerogel indicate that the CNC acts as a nano-support to reduce the deformation of the GO aerogel during the freeze-drying process. After carbonization, different degrees of shrinkage or deformation were observed for the carbon aerogels (Fig. S2, ESI†). While C–CNC–rGO and C–Lig/CNC–rGO exhibited some volume contraction in the annealing process (Fig. S2, ESI†), these volume changes were less than that observed in C–Lig–rGO. The volume change of the carbon aerogel again indicates that the presence of CNC can prevent or reduce the re-stacking of GO during annealing. Table S1† shows the density of carbon

aerogels. The density of C–CNC–rGO is 3.5 mg cm^{-3} to 4.3 mg cm^{-3}, while the density of C–Lig/CNC–rGO was slightly increased to 4.6 mg cm^{-3} to 5.7 mg cm^{-3}. However, due to the large volume reduction of C–Lig–rGO, the density of C–Lig–rGO was higher (7.9 mg cm^{-3}).

The SEM images of the carbon aerogels (Fig. 1) show that C–Lig/CNC–rGO and C–CNC–rGO have orderly, continuous, wave-like layers. However, C–Lig–rGO without CNC exhibits a disordered structure. Fig. S4† shows the TEM images of C–Lig/CNC–rGO and C–Lig–rGO, where lignin carbon dots can be seen. These carbonized lignin dots allow for interactions between adjacent rGO sheets or layers. In the Raman spectrum (Fig. S3a, ESI†), strong bands were observed around 1346 cm^{-1} and 1592 cm^{-1}, suggesting a disordered carbon structure (D band) and ordered graphite structure (G band), respectively.[32] Fig. S4b (ESI†) shows the XRD patterns of the samples. The positions and strengths of the peaks are related to the degree of graphitization. Low graphitization is suggested by the wide and low intensity peaks of C–Lig–rGO and C–CNC–rGO at $2\theta = 23.6°$.[33] The XRD pattern of C–Lig/CNC–rGO shows a slightly stronger wide peak at $2\theta = 24.8°$, which is indicative of high graphitization.[34]

Due to the brittleness of carbon, carbon aerogels often lack good compressibility and resilience. The introduction of a layered structure can improve the mechanical properties of a carbon aerogel, making it highly compressible. As shown in Fig. 1g, C–Lig–rGO exhibited remarkable plastic deformation upon compression, indicating poor elasticity, which can be attributed to the disordered structure inside the aerogel. However, C–CNC–rGO and C–Lig/CNC–rGO showed excellent elasticity and could be restored to their original height after high compression, as shown in Fig. 1e and f. In this work, the addition of CNC can maintain a stable, layered, wavy structure of carbon aerogels. Some researchers have found that wavy lamellar structures can undergo large geometric deformation.[15] When stress is applied in a direction perpendicular to the wave layers, the multi-arch structure can undergo large geometric deformation, effectively preventing collapse of the material.[15]

3.2 Mechanical performance of carbon aerogels

Fig. 2 shows the elasticity of carbon aerogels. From Fig. 2a, it can be seen that the height of C–CNC–rGO can recover to its original height after 10%, 30% and 50% compression strain, but when the compression strain is 80%, 90%, the height has

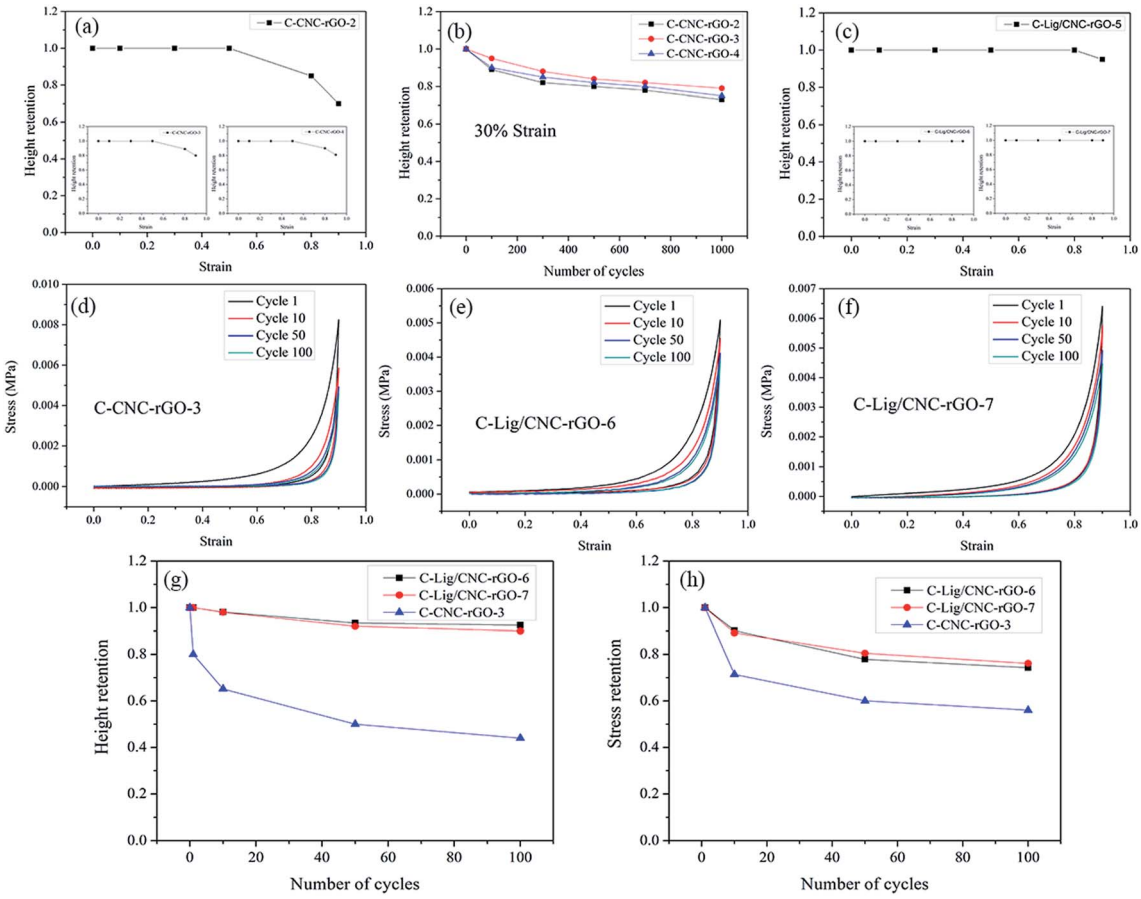

Fig. 2 (a) Height retention of C–CNC–rGO under different compression strains. (b) Height retention of C–CNC–rGO after 1000 cycles of 30% strain. (c) Height retention of C–Lig/CNC–rGO under different compression strains. Stress–strain plots of (d) C–CNC–rGO-3 (e) C–Lig/CNC–rGO-6 and (f) C–Lig/CNC–rGO-7 at a strain of 90% for 100 cycles. (g) The height retention of C–CNC–rGO-3, C–Lig/CNC–rGO-6 and C–Lig/CNC–rGO-7 at a strain of 90% for 100 cycles. (h) The stress retention of C–CNC–rGO-3, C–Lig/CNC–rGO-6 and C–Lig/CNC–rGO-7 at a strain of 90% for 100 cycles.

dropped and failed to return to its original height. The carbon aerogel's height retention rate increased with the increase in the amount of CNC in the sample. When the concentration of CNC was 2 mg mL^{-1}, the carbon aerogel's height retention rate was 69.5% under 90% compression deformation, and the amount of CNC added at 4 mg mL^{-1} and 6 mg mL^{-1}, the carbon aerogel has a height retention rate of 81% and 80% under 90% compression deformation. Fig. 2b shows the altitude retention rate of C–CNC–rGO after 1000 cycles under 30% strain. C–CNC–rGO has a maximum height retention rate of 79% after 30% 1000 cycles. Fig. 2c shows the height retention of the C–Lig/CNC–rGO once cycled under different compression deformations. It can be seen that when the added of lignin is 0.4 mg mL^{-1}, the height of the carbon aerogel does not decrease after compressive strain of 10–80%, and the height of the carbon aerogel is 95% of the original after 90% compressive strain. When the amount of lignin is 2 mg mL^{-1} and 4 mg mL^{-1}, C–Lig/CNC–rGO-6 and C–Lig/CNC–rGO-7 can return to their original height after 10–90% compressive strain. The above results can show that the addition of lignin significantly improves the resilience of carbon aerogels. Due to the interlayer interaction caused by carbonization of lignin, C–Lig/CNC–rGO has a more stable structure and higher mechanical compressive strength. Fig. 2d–f are compressive stress–strain curves of C–CNC–rGO-3, C–Lig/CNC–rGO-6, and C–Lig/CNC–rGO-7 at a strain of 90% for 100 cycles. The presence of hysteresis loops in the sample indicates that the mechanical response of the carbon aerogel during compression is viscoelastic behavior. This behavior occurs on almost all compressible carbon.[28] At a high strain of 90%, the height of C–CNC–rGO-3 decreased significantly, and the height remained at 40% after 100 cycles (Fig. 2g). Fig. 2e shows that C–Lig/CNC–rGO-6 showed no loss of height at 90% strain after 1 compression cycle and only 2% height loss after 10 compression cycles. Even after 90% strain for 100 cycles, C–Lig/CNC–rGO-6 could recover 92% of its original height. C–Lig/CNC–rGO-7 could recover 90% of its original height after 90% strain for 100 cycles. As can be seen from Fig. 2h, the stress of C–CNC–rGO-3 at 90% deformation decreased to 71.0% at the 10th cycle, and the stress retention at the 50th and 100th cycles decreased significantly to 59.4% and 55.6%, respectively. Under the 90% strain condition, the stress retention of C–Lig/CNC–rGO-6 and C–Lig/CNC–rGO-7 after 100 cycles was 72% and 74%, which was even higher than the stress retention of C–CNC–rGO-3 after 1 cycle.

Fig. 3 shows the supercompressibility and fatigue resistance of C–Lig/CNC–rGO-6. The continuous and undulating rGO layers allow for high compression. The C–Lig/CNC–rGO-6 sample could withstand an extreme strain of 99%, as shown in Fig. 3a. As shown in Fig. 3b and c, the height retention and stress retention of C–Lig/CNC–rGO-6 were 73.5% and 85%, respectively, at an extreme 99% strain for 10 cycles. Fig. 3d shows the high fatigue resistance of C–Lig/CNC–rGO-6 at up to 10 000 cycles at 30% strain. The interactions between the rGO layers produced by the carbonization of the CNC and lignin can produce a flexible layer, and thus provide the aerogel with excellent fatigue resistance. As shown in Fig. 3e, C–Lig/CNC–rGO-6 almost completely recovered its height after 2000 cycles at 30% strain, and its height was 97% of the initial height after 3000 cycles. Furthermore, the height retention only slightly decreased to 91.3% after 10 000 cycles. As can be seen from Fig. 3f, the stress of the C–Lig/CNC–rGO-6 aerogel dropped to 95.8% at the 10 000th cycle at 30% strain. The ultra-stable structure of C–Lig/CNC–rGO results in its high stress retention. The mechanical properties of C–Lig/CNC–rGO-6 are superior to other compressible carbon materials such as silicone sponges,[35] carbonaceous nanofibrous aerogels,[13]

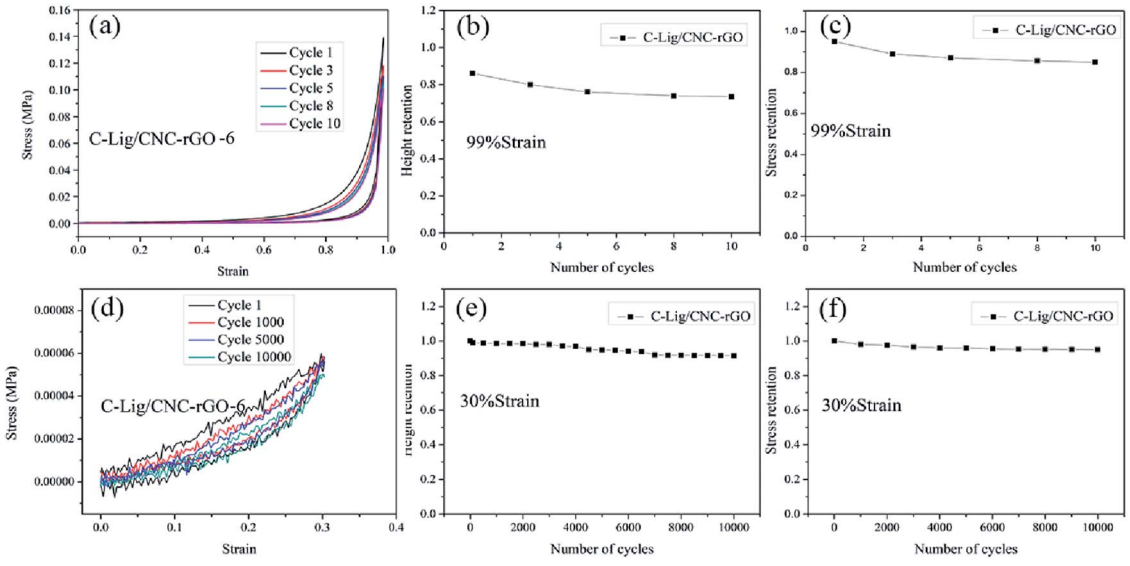

Fig. 3 Supercompressibility, elasticity, and fatigue resistance of C–Lig/CNC–rGO-6. (a) Stress–strain plots of C–Lig/CNC–rGO-6 at a strain of 99% for 10 cycles. (b) Height retention of C–Lig/CNC–rGO at a strain of 99% for 10 cycles. (c) Stress retention of C–Lig/CNC–rGO-6 at a strain of 99% for 10 cycles. (d) Stress–strain plots of C–Lig/CNC–rGO-6 at a strain of 30% for 10 000 cycles. (e) Height retention of C–Lig/CNC–rGO-6 at a strain of 30% for 10 000 cycles. (f) Stress retention of C–Lig/CNC–rGO-6 at a strain of 30% for 10 000 cycles.

polyimide-graphene aerogels,[36] nanofibrous aerogels,[37] and graphene aerogels,[38] as shown in Table S2 (ESI†). These results emphasize the superior mechanical properties of the C–Lig/CNC–rGO-6 aerogel due to its continuous, wavy, layered structure and the interactions between CNC and lignin in the enhanced rGO layer.

3.3 Strain and electrical signal response of carbon aerogels

Fig. 4a shows the current responses of C–Lig/CNC–rGO-6 at different compressive strains (at a voltage of 1 V). It can be seen from the figure that the current in C–Lig/CNC–rGO-6 increased rapidly upon compression and decreased rapidly upon release. The current intensity increased from 0.0001 A to 0.045 A as the compressive strain was increased from 10% to 90%. This is because the change in contact resistance of the material conductive block affects the conductivity of the material. The larger the interlayer contact area of the carbon aerogel at the time of compression, the smaller the electric resistance and the higher the conductivity. In order to investigate the current response stability of C–Lig/CNC–rGO-6, we recorded the compression cycle electrical signals of carbon aerogels at different strains. As shown in Fig. 4b, C–Lig/CNC–rGO-6 was cycled 10 000 times at 30% high strain, and the current change was very stable with almost no attenuation after 10 000 cycles. Surprisingly, C–Lig/CNC–rGO-6 performed well for 100 cycles at 90% strain; the current slightly decreased during the initial 10 cycles and then became stable over the following cycles. The current response stability of C–Lig/CNC–rGO-6 can be attributed to its highly stable mechanical properties.

Fig. 4d shows the sensitivity of C–Lig/CNC–rGO-6. The sensitivity is calculated according to eqn (1).

$$S = \delta(\Delta I/I_0)/\delta P \quad (1)$$

where ΔI and I_0 are the change in the current and initial current without applied pressure, respectively, and δP is the pressure change. It is worth noting that the sensitivity of C–Lig/CNC–rGO-6 was high, reaching 86.41 kPa^{-1}, and exhibited a wide linear range (a stress of 3.5 kPa relates to 80% strain of C–Lig/CNC–rGO-6, Fig. 4d), indicating that the aerogel can provide an accurate output signal. Fig. 4d reveals a stable and sensitive relationship between the applied pressure and the electrical signal output. As shown in Table S2,† the ultra-high and wide-range linear sensitivity of C–Lig/CNC–rGO-6 is superior to flexible substrate-loaded carbon,[39–42] sensitive films,[43–45] 3D carbon materials,[46–48] and other common materials. Fig. 4g shows the pressure detection limits for the C–Lig/CNC–rGO-6 aerogel. A high-sensitivity sensor was fabricated by assembling a carbon aerogel between two Au electrodes adhered to a polyethylene terephthalate (PET) substrate. The sensor was able to detect small changes in pressure with a detection limit as low as 0.875

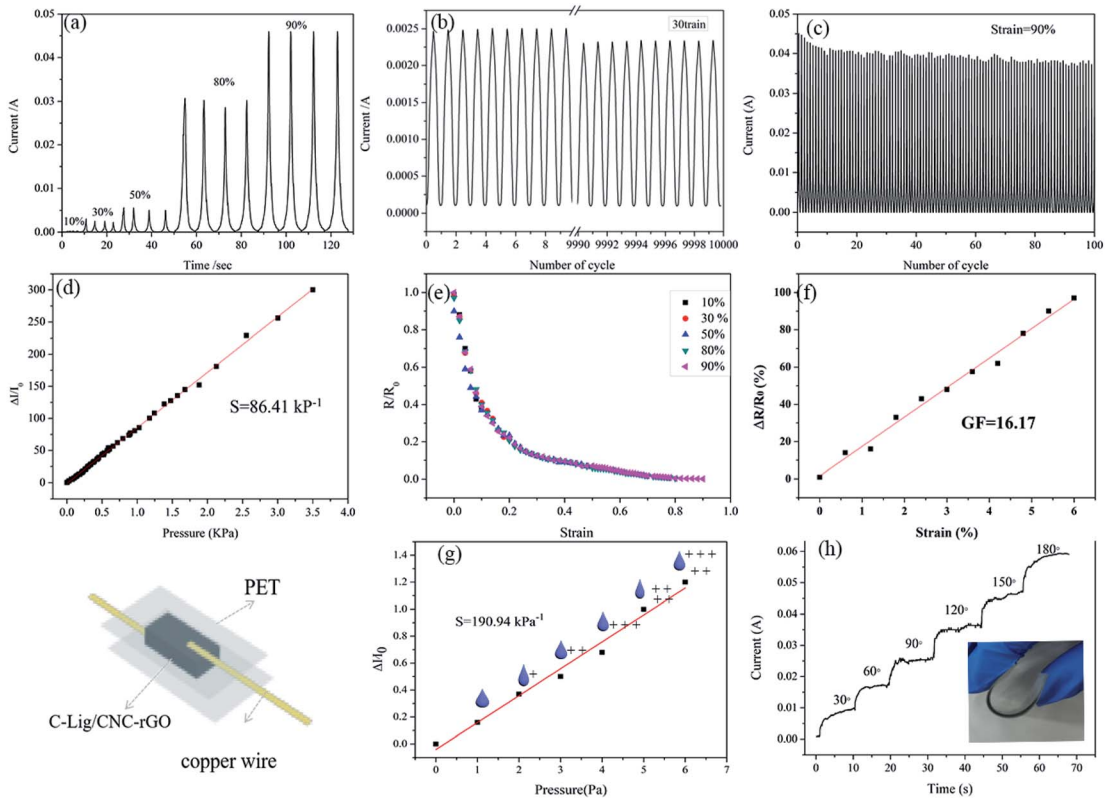

Fig. 4 Strain and electrical signal response of C–Lig/CNC–rGO-6. (a) Current at different strains of C–Lig/CNC–rGO-6. (b) Current response for 10 000 cycles at 30% strain. (c) Current response for 100 cycles at 90% strain. (d) Ultrahigh linear sensitivity of stress from 0 to 3.5 kPa. (e) Normalized resistance R/R_0 at different strains. (f) The gauge factor at strains from 0 to 6%. (g) Ultrahigh sensitivity for detecting tiny load. (h) Current at different bending angles.

Pa (50 μL water droplets). The current increased as the number of water droplets was increased. In the region of pressure ≤ 6 Pa, the current and stress maintained a good linear relationship with a sensitivity of up to 190.94 kPa^{-1}. These results demonstrate the ultra-low detection limit and high sensitivity of the carbon aerogel.

Another important parameter for characterizing sensor sensitivity is the gauge factor (GF). The gauge factor (GF) reflecting strain sensitivity can be expressed by eqn (2)

$$GF = \delta(\Delta R/R_0)/\delta\varepsilon \quad (2)$$

where ΔR is the change in resistance with compression strain, R_0 is the resistance before strain, and ε is the applied strain. The normalized resistance (R/R_0) curves of C–Lig/CNC–rGO-6 at different strains are almost the same, as shown in Fig. 4e. These results indicate that C–Lig/CNC–rGO-6 has an ultra-stable structure. When the strain was less than 10%, the contact area of the C–Lig/CNC–rGO-6 carbon layer increased rapidly, leading to a linear drop in normalized resistance. Fig. 4f shows that C–Lig/CNC–rGO-6 exhibited a GF of 16.17 within 5% strain, which makes the C–Lig/CNC–rGO-6 an ideal strain sensor. In addition, the sensor can be repeatedly bent from 0° to 180° (Fig. 4h), and the conductivity of the sensor increases as the bending angle increases. The compressive force generated when the carbon aerogel is bent causes an increase in the contact area between the wavy layers, and thus the electrical resistance is lowered. These properties make the C–Lig/CNC–rGO-6 an ideal sensor material.

3.4 Application of carbon aerogels as a wearable sensor

Benefiting from its excellent mechanical performance, stable current response, and high sensitivity, C–Lig/CNC–rGO can be

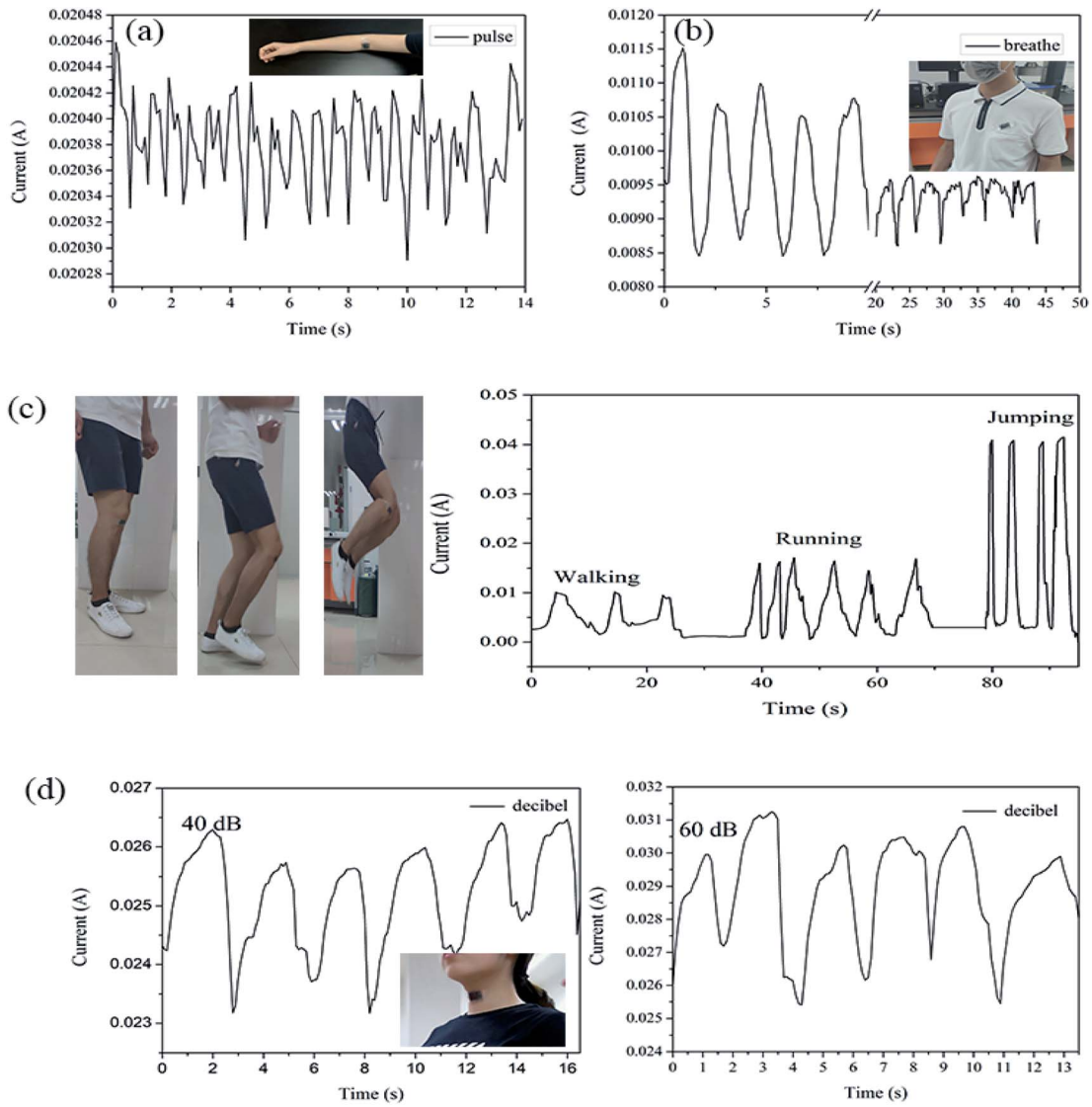

Fig. 5 Applications of C–Lig/CNC–rGO–6 for body motion recognition and biosignal detection. (a) The output current change of the sensor in response to the pulse of an arm artery. (b) The output current of the sensor varies with the respiration of the human body. (c) The response of the output current to knee flexion. (d) The current signals from sounds of 60 decibels and 40 decibels.

attached to the human body as a wearable device to detect biosignals. Fig. 5 illustrates the change in current when the wearable device records data from the human body. The sensor can record the pulse of the human body. As displayed in Fig. 5a, a pulse wave of 81 beats per min can be seen when the sensor is attached to the wrist of an adult who is resting. It can be found that the current difference caused by pulse vibration is 0.8 mA, which is higher than the current difference caused by other graphene oxide carbon aerogels under the same conditions, such as C–CNC/rGO–glu2 carbon aerogel prepared by Zhuo *et al.* (0.4 mA).[49] C–Lig/CNC–rGO can also capture human motion signals. As shown in Fig. 5b, the respiratory rates of the human body during running and resting were measured at 2 s per time and 3.5 s per time, respectively. The sensor also records the motion signal of the knee joint (Fig. 5c). In addition, it can clearly detect the vibration of the throat when speaking at different levels, such as 60 decibels and 40 decibels (Fig. 5d). These results indicate that the wearable sensor prepared using C–Lig/CNC–rGO has broad application prospects in detecting human motion.

4. Conclusions

A carbon aerogel with high mechanical properties and high sensitivity was successfully prepared by using cellulose and lignin to increase the interaction between graphene oxide layers. The prepared carbon aerogel has high mechanical properties such as super compressibility, excellent elasticity and good fatigue resistance. The linear sensitivity of the carbon aerogel in the range of 0 3.5 kPa is 86.41 kPa, and the sensitivity (0.6 Pa) under minute pressure is 190.94 kPa^{-1}. These excellent properties make this carbon aerogel ideal for pressure sensors. The assembled sensor has good sensitivity to small signals such as water droplets and human pulse. The prepared carbon aerogel has good application prospects in wearable devices.

Conflicts of interest

There are no conflicts to declare.

Acknowledgements

This work was financially supported by the Guangxi Natural Science Foundation (2017GXNSFAA198220 & 2018GXNSFAA294074) and the Scientific Research Foundation of Guangxi University (XJZ160945).

References

1 Y. J. Hu, H. Zhuo, Z. H. Chen, K. Z. Wu, Q. S. Luo, Q. Z. Liu, S. S. Jing, C. F. Liu, L. X. Zhong, R. C. Sun and X. W. Peng, Superelastic Carbon Aerogel with Ultrahigh and Wide-Range Linear Sensitivity, *ACS Appl. Mater. Interfaces*, 2018, **10**(47), 40641–40650.

2 T. Chen, J. Zhang, P. H. Shi, Y. Li, L. Zhang, Z. Z. Sun, R. He, T. Duan and W. K. Zhu, Thalia dealbata Inspired Anisotropic Cellular Biomass Derived Carbonaceous Aerogel, *ACS Sustainable Chem. Eng.*, 2018, **6**(12), 17152–17159.

3 Y. A. Samad, Y. Q. Li, A. Schiffer, S. M. Alhassan and K. Liao, Graphene Foam Developed with a Novel Two-Step Technique for Low and High Strains and Pressure-Sensing Applications, *Small*, 2015, **11**(20), 2380–2385.

4 C. Y. Yan, J. X. Wang, W. B. Kang, M. Q. Cui, X. Wang, C. Y. Foo, K. J. Chee and P. S. Lee, Highly Stretchable Piezoresistive Graphene-Nanocellulose Nanopaper for Strain Sensors, *Adv. Mater.*, 2014, **26**(13), 2022–2027.

5 M. C. Zhang, C. Y. Wang, H. M. Wang, M. Q. Jian, X. Y. Hao and Y. Y. Zhang, Carbonized Cotton Fabric for High-Performance Wearable Strain Sensors, *Adv. Funct. Mater.*, 2017, **27**(2), 1604795.

6 M. Wang, C. Y. Shao, S. K. Zhou, J. Yang and F. Xu, Super-compressible, fatigue resistant and anisotropic carbon aerogels for piezoresistive sensors, *Cellulose*, 2018, **25**(12), 7329–7340.

7 F. Guo, Y. Q. Jiang, Z. Xu, Y. H. Xiao, B. Fang, Y. J. Liu, W. W. Gao, P. Zhao, H. T. Wang and C. Gao, Highly stretchable carbon aerogels, *Nat. Commun.*, 2018, **9**(1), 881.

8 Y. Wu, N. Yi, L. Huang, T. Zhang, S. Fang, H. Chang, N. Li, J. Oh, J. A. Lee and M. Kozlov, Three-dimensionally bonded spongy graphene material with super compressive elasticity and near-zero Poisson's ratio, *Nat. Commun.*, 2015, **6**, 6141.

9 I. K. Moon, S. Yoon, K. Y. Chun and J. Oh, Highly Elastic and Conductive N-Doped Monolithic Graphene Aerogels for Multifunctional Applications, *Adv. Funct. Mater.*, 2016, **25**(45), 6954.

10 Y. Li, J. Chen, L. Huang, C. Li, J.-D. Hong and G. Shi, Highly Compressible Macroporous Graphene Monoliths via an Improved Hydrothermal Process, *Adv. Mater.*, 2014, **26**(28), 4789–4793.

11 K. H. Kim, M. N. Tsui and M. F. Islam, Graphene-Coated Carbon Nanotube Aerogels Remain Superelastic while Resisting Fatigue and Creep over −100 to +500 degrees C, *Chem. Mater.*, 2017, **29**(7), 2748–2755.

12 H. Zhang, J. Feng, L. Li, Y. Jiang and J. Feng, Controlling the microstructure of resorcinol–furfural aerogels and derived carbon aerogels via the salt templating approach, *RSC Adv.*, 2019, **9**(11), 5967–5977.

13 Y. Si, X. Wang, C. Yan, L. Yang, J. Yu and B. Ding, Ultralight Biomass-Derived Carbonaceous Nanofibrous Aerogels with Superelasticity and High Pressure-Sensitivity, *Adv. Mater.*, 2016, **28**(43), 9655.

14 L. Qiu, J. Z. Liu, S. L. Y. Chang, Y. Wu and D. Li, Biomimetic superelastic graphene-based cellular monoliths, *Nat. Commun.*, 2012, **3**(4), 1241.

15 H. L. Gao, Y. B. Zhu and L. B. Mao, Super-elastic and fatigue resistant carbon material with lamellar multi-arch microstructure, *Nat. Commun.*, 2016, **7**, 12920.

16 H. Bai, Y. Chen, B. Delattre, A. P. Tomsia and R. O. Ritchie, Bioinspired large-scale aligned porous materials assembled with dual temperature gradients, *Sci. Adv.*, 2015, **1**(11), e1500849.

17 H. Wang, W. Lu, J. Di, D. Li, X. Zhang, M. Li, Z. Zhang, L. Zheng and Q. Li, Ultra-Lightweight and Highly Adaptive All-Carbon Elastic Conductors with Stable Electrical Resistance, *Adv. Funct. Mater.*, 2017, **27**(13), 1606220.

18 C. Chen, F. Li, Y. Zhang, B. Wang, Y. Fan, X. Wang and R. Sun, Compressive, ultralight and fire-resistant lignin-modified graphene aerogels as recyclable absorbents for oil and organic solvents, *Chem. Eng. J.*, 2018, **350**, 173–180.

19 C. Li, D. Jiang, H. Liang, B. Huo, C. Liu, W. Yang and J. Liu, Superelastic and Arbitrary-Shaped Graphene Aerogels with Sacrificial Skeleton of Melamine Foam for Varied Applications, *Adv. Funct. Mater.*, 2017, **28**(8), 1704674.

20 Z. Ma, A. Wei, J. Ma, L. Shao, H. Jiang, D. Dong, Z. Ji, Q. Wang and S. Kang, Lightweight, compressible and electrically conductive polyurethane sponges coated with synergistic multiwalled carbon nanotubes and graphene for piezoresistive sensors, *Nanoscale*, 2018, **10**(15), 7116–7126.

21 J. P. Zhang, B. C. Li, L. X. Li and A. Q. Wang, Ultralight, compressible and multifunctional carbon aerogels based on natural tubular cellulose, *J. Mater. Chem. A*, 2016, **4**(6), 2069–2074.

22 C. Li, Z.-Y. Wu, H.-W. Liang, J.-F. Chen and S.-H. Yu, Ultralight Multifunctional Carbon-Based Aerogels by Combining Graphene Oxide and Bacterial Cellulose, *Small*, 2017, **13**(25), 1700453.

23 C. S. Boland, U. Khan, G. Ryan, S. Barwich, R. Charifou, A. Harvey, C. Backes, Z. Li, M. S. Ferreira and M. E. Mobius, Sensitive electromechanical sensors using viscoelastic graphene-polymer nanocomposites, *Science*, 2016, **354**(6317), 1257–1260.

24 T. Chen, J. Zhang, P. Shi, Y. Li, L. Zhang, Z. Sun, R. He, T. Duan and W. Zhu, Thalia dealbata Inspired Anisotropic Cellular Biomass Derived Carbonaceous Aerogel, *ACS Sustainable Chem. Eng.*, 2018, **6**(12), 17152–17159.

25 X. Peng, K. Wu, Y. Hu, H. Zhuo, Z. Chen, S. Jing, Q. Liu, C. Liu and L. Zhong, A mechanically strong and sensitive CNT/rGO–CNF carbon aerogel for piezoresistive sensors, *J. Mater. Chem. A.*, 2018, **6**(46), 23550–23559.

26 W. S. Hummers and R. E. Offeman, Preparation of Graphitic Oxide, *J. Am. Chem. Soc.*, 1958, **80**(6), 1339.

27 X. Liu, S. Shi, Y. Li, J. Forth, D. Wang and T. P. Russell, Liquid Tubule Formation and Stabilization Using Cellulose Nanocrystal Surfactants, *Angew. Chem.*, 2017, **56**(41), 12594.

28 H. Zhuo, Y. Hu, X. Tong, Z. Chen, L. Zhong, H. Lai, L. Liu, S. Jing, Q. Liu and C. Liu, A Supercompressible, Elastic, and Bendable Carbon Aerogel with Ultrasensitive Detection Limits for Compression Strain, Pressure, and Bending Angle, *Adv. Mater.*, 2018, **30**(18), 1706705.

29 L. Zhang, H. Lu, J. Yu, E. McSporran, A. Khan, Y. Fan, Y. Yang, Z. Wang and Y. Ni, Preparation of High-Strength Sustainable Lignocellulose Gels and Their Applications for Antiultraviolet Weathering and Dye Removal, *ACS Sustainable Chem. Eng.*, 2019, **7**(3), 2998–3009.

30 Y. Peng, S. S. Nair, H. Chen, N. Yan and J. Cao, Effects of lignin content on mechanical and thermal properties of polypropylene composites reinforced with micro particles of spray dried cellulose nanofibrils, *ACS Sustainable Chem. Eng.*, 2018, **6**(8), 11078–11086.

31 H. L. Gao, Y. B. Zhu, L. B. Mao, F. C. Wang, X. S. Luo, Y. Y. Liu, Y. Lu, Z. Pan, J. Ge, W. Shen, Y. R. Zheng, L. Xu, L. J. Wang, W. H. Xu, H. A. Wu and S. H. Yu, Super-elastic and fatigue resistant carbon material with lamellar multi-arch microstructure, *Nat. Commun.*, 2016, **7**, 12920.

32 B. Murugesan, N. Pandiyan, M. Arumugam, M. Veerasingam, J. Sonamuthu, A. R. Jeyaraman, S. Samayanan and S. Mahalingam, Two dimensional graphene oxides converted to three dimensional P, N, F and B, N, F tri-doped graphene by ionic liquid for efficient catalytic performance, *Carbon*, 2019, **151**, 53–67.

33 F. Su, C. K. Poh, J. S. Chen, G. Xu, W. Dan, L. Qin, J. Lin and W. L. Xiong, Nitrogen-containing microporous carbon nanospheres with improved capacitive properties, *Energy Environ. Sci.*, 2011, **4**(3), 717–724.

34 M. Biswal, A. Banerjee, M. Deo and S. Ogale, From dead leaves to high energy density supercapacitors, *Energy Environ. Sci.*, 2013, **6**(4), 1249–1259.

35 L. Li, T. Hu, Y. Yang and J. Zhang, Strong, compressible, bendable and stretchable silicone sponges by solvent-controlled hydrolysis and polycondensation of silanes, *J. Colloid Interface Sci.*, 2019, **540**, 554–562.

36 R.-P. Ren, Z. Wang, J. Ren and Y.-K. Lv, Highly compressible polyimide/graphene aerogel for efficient oil/water separation, *J. Mater. Sci.*, 2019, **54**(7), 5918–5926.

37 Y. Si, J. Yu, X. Tang, J. Ge and B. Ding, Ultralight nanofibre-assembled cellular aerogels with superelasticity and multifunctionality, *Nat. Commun.*, 2014, **5**, 5802.

38 C. Wang, X. Chen, B. Wang, M. Huang and R. S. Ruoff, Freeze-Casting Produces a Graphene Oxide Aerogel with a Radial and Centrosymmetric Structure, *ACS Nano*, 2018, **12**(6), 5816–5825.

39 Y. Si, X. Q. Wang, C. C. Yan, L. Yang, J. Y. Yu and B. Ding, Ultralight Biomass-Derived Carbonaceous Nanofibrous Aerogels with Superelasticity and High Pressure-Sensitivity, *Adv. Mater.*, 2016, **28**(43), 9512–9518.

40 X. D. Wu, Y. Y. Han, X. X. Zhang, Z. H. Zhou and C. H. Lu, Large-Area Compliant, Low-Cost, and Versatile Pressure-Sensing Platform Based on Microcrack-Designed Carbon Black@Polyurethane Sponge for Human-Machine Interfacing, *Adv. Funct. Mater.*, 2016, **26**(34), 6246–6256.

41 M. Q. Jian, K. L. Xia, Q. Wang, Z. Yin, H. M. Wang, C. Y. Wang, H. H. Xie, M. C. Zhang and Y. Y. Zhang, Flexible and Highly Sensitive Pressure Sensors Based on Bionic Hierarchical Structures, *Adv. Funct. Mater.*, 2017, **27**(9), 1606066.

42 X. W. Wang, Y. Gu, Z. P. Xiong, Z. Cui and T. Zhang, Silk-Molded Flexible, Ultrasensitive, and Highly Stable Electronic Skin for Monitoring Human Physiological Signals, *Adv. Mater.*, 2014, **26**(9), 1336–1342.

43 C. Y. Hou, H. Z. Wang, Q. H. Zhang, Y. G. Li and M. F. Zhu, Highly Conductive, Flexible, and Compressible All-Graphene Passive Electronic Skin for Sensing Human Touch, *Adv. Mater.*, 2014, **26**(29), 5018–5024.

44 Z. G. Qiu, Y. B. Wan, W. H. Zhou, J. Y. Yang, J. L. Yang, J. Huang, J. M. Zhang, Q. X. Liu, S. Y. Huang, N. N. Bai, Z. G. Wu, W. Hong, H. Wang and C. F. Guo, Ionic Skin with Biomimetic Dielectric Layer Templated from Calathea Zebrine Leaf, *Adv. Funct. Mater.*, 2018, **28**(37), 1802343.

45 L. Z. Sheng, Y. Liang, L. L. Jiang, Q. Wang, T. Wei, L. T. Qu and Z. J. Fan, Bubble-Decorated Honeycomb-Like Graphene Film as Ultrahigh Sensitivity Pressure Sensors, *Adv. Funct. Mater.*, 2015, **25**(41), 6545–6551.

46 J. L. Xiao, Y. Q. Tan, Y. H. Song and Q. Zheng, A flyweight and superelastic graphene aerogel as a high-capacity adsorbent and highly sensitive pressure sensor, *J. Mater. Chem. A*, 2018, **6**(19), 9074–9080.

47 Y. N. Ma, Y. Yue, H. Zhang, F. Cheng, W. Q. Zhao, J. Y. Rao, S. J. Luo, J. Wang, X. L. Jiang, Z. T. Liu, N. S. Liu and Y. H. Gao, 3D Synergistical MXene/Reduced Graphene Oxide Aerogel for a Piezoresistive Sensor, *ACS Nano*, 2018, **12**(4), 3209–3216.

48 X. W. Peng, K. Z. Wu, Y. J. Hu, H. Zhuo, Z. H. Chen, S. S. Jing, Q. Z. Liu, C. F. Liu and L. X. Zhong, A mechanically strong and sensitive CNT/rGO–CNF carbon aerogel for piezoresistive sensors, *J. Mater. Chem. A*, 2018, **6**(46), 23550–23559.

49 H. Zhuo, Y. J. Hu, X. Tong, Z. H. Chen, L. X. Zhong, H. H. Lai, L. X. Liu, S. S. Jing, Q. Z. Liu, C. F. Liu, X. W. Peng and R. C. Sun, A Supercompressible, Elastic, and Bendable Carbon Aerogel with Ultrasensitive Detection Limits for Compression Strain, Pressure, and Bending Angle, *Adv. Mater.*, 2018, **30**(18), 1706705.